



# On-demand pitch tuning of printed chiral nematic liquid crystal droplets

Waqas Kamal, Alva C.J. Orr, Thomas C. Sykes, Alfonso A. Castrejón-Pita, Steve J. Elston, Stephen M. Morris<sup>\*</sup>

Department of Engineering Science, University of Oxford, Parks Road, Oxford, OX1 3PJ, UK

## ARTICLE INFO

### Keywords:

Inkjet printing  
Chiral nematic liquid crystals  
Cholesterics  
Reflection band  
Drop-on-demand

## ABSTRACT

Identifying facile means with which to tune the pitch of, and therefore the reflected colour from, chiral nematic liquid crystals (CLC) is of interest for many different photonics applications including optical filters, coloured displays, and mirrorless lasers. Precise control of the pitch of the helix, however, can be challenging. Here, we demonstrate the ability to tune the pitch, and consequently the reflection band, by depositing picolitre volumes of nematic LC into printed CLC droplets with a short pitch. Results are presented that demonstrate mixing of the nematic LC and CLC droplets such that the pitch elongates causing the reflection band located at blue wavelengths (430 nm) to redshift to longer wavelengths. The magnitude of the redshift can be controlled by varying the number of nematic LC droplets deposited into each CLC droplet. We consider the process of diffusion of these two separate mixtures using inkjet printing and showcase how this process of tuning the pitch can be employed to create coloured images in the form of an alphanumeric logo.

## 1. Introduction

There has long been an interest to develop different methods with which to tune the selective reflection band of chiral nematic liquid crystals (CLCs). The reflection band of a CLC is centered at the wavelength  $\lambda_c = \bar{n}P$  where  $P$  denotes the pitch, defined as the length scale across which the helix completes a full revolution, and  $\bar{n}$  represents the average refractive index of the LC [1,2]. The pitch and average refractive index of CLCs have been demonstrated to be influenced by a range of external stimuli, including light [3–5], temperature [6,7], electric field [8–10], mechanical force [11,12], humidity [13,14], and chemical fumes [15–17]. These dependencies suggest that the reflection band of CLCs can be easily modulated through the application of such external stimuli, thereby offering potential for a diverse range of applications, including filters [18,19], sensors [7,20], tunable colour reflectors [21,22], and light shutters [23,24].

Traditionally, CLCs devices typically consist of a thin layer of liquid crystalline material sandwiched between glass substrates. However, there has been a great deal of interest in processing LC materials as freestanding inkjet printed microdroplets, due to their potential for increased flexibility and scalability compared to conventional thin film-based devices. For instance, Gardiner et al. showcased uniform arrays of dye-doped CLCs for printed lasers [25]. Additionally, we have demonstrated the spatial patterning of polymer-stabilized CLCs and

polymer-dispersed LCs in the form of pixels for printed smart window technologies [26,27]. Similarly, Monali et al. as well as Yang et al. have reported an interesting approach in three separate studies to locally tune the reflected colour of a pre-coated CLC polymer film. In their work, tuning has been achieved by spatially printing a nematic LC or an aqueous solution as an ink, thereby changing the pitch and consequently tuning the reflected colour [28–30]. In contrast, Lei et al. utilized four distinct ink compositions to demonstrate spatial patterning of CLC droplets, which generated fluorescent and structural colour when illuminated with and without ultraviolet light, respectively [31]. These research findings by Lei et al. exemplify the promising application of inkjet printing for the fabrication of printed coloured LC reflectors. However, the approach presented therein was limited by the need to prepare separate CLC compositions for blue, green, and red reflection, and then to subsequently print them individually in relatively large diameters (1 mm in diameter). Combined, such a process could impede the practical implementation of printed CLC microdroplet-based technologies. In particular, the need to prepare individual mixtures before printing limits the process to a fixed subset of colours. Furthermore, the study does not provide detailed optical characterisation of a single droplet when observed from both sides of the assembled device.

In the present study, we introduce an innovative method to adjust the reflection colour of printed short-pitch CLC droplets by depositing, in a drop-on-demand (DoD) fashion, achiral nematic LC droplets into

<sup>\*</sup> Corresponding author.

E-mail address: [stephen.morris@eng.ox.ac.uk](mailto:stephen.morris@eng.ox.ac.uk) (S.M. Morris).

<https://doi.org/10.1016/j.mtadv.2023.100416>

Received 30 May 2023; Received in revised form 9 August 2023; Accepted 14 August 2023

Available online 23 August 2023

2590-0498/© 2023 The Authors. Published by Elsevier Ltd. This is an open access article under the CC BY license (<http://creativecommons.org/licenses/by/4.0/>).

them. The scalability enabled by DoD inkjet printing permits precise volume depositions of nematic LC in the form of picolitre droplets, resulting in the formation of longer-pitch droplets that subsequently reflect light at extended wavelengths. By digitally controlling the pitch in this manner, we demonstrate the fabrication of a comprehensive library of CLC-based colours, indicating a novel means of tuning the pitch of CLC droplets across large wavelength ranges so as to reflect a diverse colour palette. Finally, we demonstrate the practical feasibility of this technique by spatially tuning the reflected colour from CLC droplets that form three alphabetical characters.

## 2. Materials and methods

### 2.1. The CLC ink

An initial short-pitch CLC mixture was formed by doping a eutectic nematic mixture, E7 (Synthon Chemicals Ltd), henceforth generally referred to as the nematic LC (NLC), with a chiral dopant, BDH1281 (Merck KGaA). E7 was chosen as the host material owing to its compatibility with Drop-on-Demand (DoD) printing [32,33] and

because it exhibits a nematic phase at room temperature. Since the aim of this study is to generate droplets with pitches of the order of the wavelength of visible light, a chiral dopant with a sufficiently high helical twisting power (HTP) was needed. BDH1281 was chosen because its HTP is  $75.6 \mu\text{m}^{-1}$ , which meant that CLC mixtures with pitches in the range of 300–500 nm could be obtained with a relatively low concentration of dopant (by weight percentage), reducing any potential adverse effects the dopant may have on the printability of the CLC. To prepare the initial mixture, 4.7 wt% of BDH1281 was added to E7 and mixed at  $68^\circ\text{C}$  for 24 h. The resultant chiral nematic mixture, which was found to reflect blue light, is henceforth referred as the CLC mixture.

### 2.2. Printing process

The process for tuning the CLC droplet reflectors using DoD printing is shown in Fig. 1. The first stage in preparing the samples was printing the initial, short-pitch CLC droplets using a MicroFab JetLab II printer (Step i) in Fig. 1). Commercially available empty glass cells of 20  $\mu\text{m}$  spacing thickness (LC2, INSTEC) with rubbed polyimide alignment layers were carefully disassembled and one of the glass substrates was

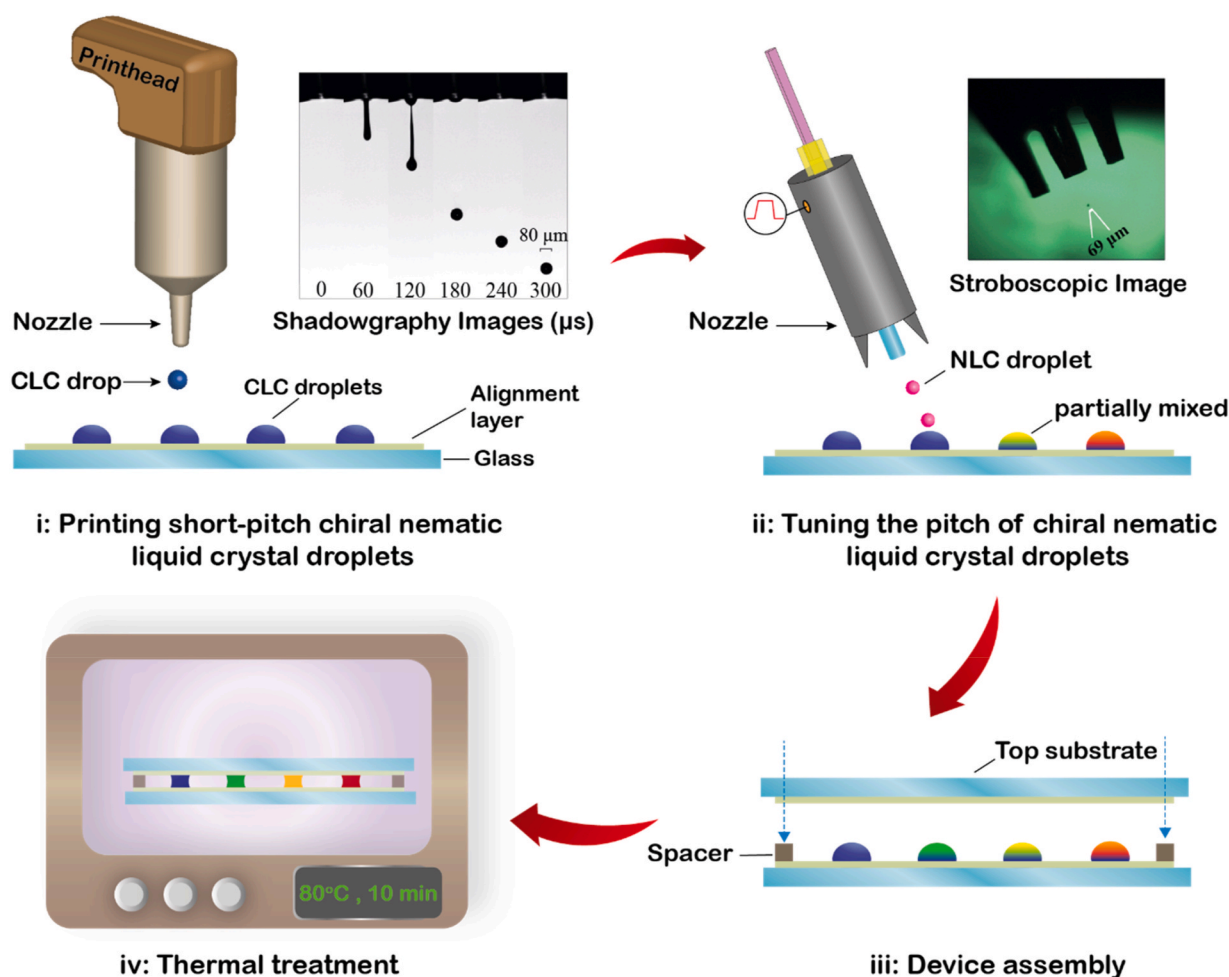


**Fig. 1.** Process for tuning the CLC pitch through inkjet printing of a NLC. An illustration depicting the steps followed to tune the pitch of printed short-pitch chiral nematic liquid crystal (CLC) droplets by depositing nematic liquid crystal (NLC) droplets at various concentrations on top of the printed CLCs. i) Printing of short pitch CLC droplets using a MicroFab JetLab II inkjet printer equipped with an 80  $\mu\text{m}$  internal diameter nozzle. The series of shadowgraph images displayed as an inset shows the fluid ejection from the nozzle, the pinch off and formation of a droplet at different timescales. ii) Depositing nematic LC droplets into the printed short-pitch CLC droplets to change the reflected colour from each droplet. The colour gradient within the droplets indicates the partial mixing of the NLC when first printed into the short pitch CLC droplets. A bespoke inkjet printer equipped with an 80  $\mu\text{m}$  internal diameter and high-speed colour camera was used to record the deposition of the droplets. The shadowgraph image on the right shows successful NLC droplet generation, without the formation of any satellite droplets. iii) Application of a top glass substrate onto the printed and diluted CLC droplets. iv) Heating the assembled device in an oven to encourage the diffusion of the printed nematic LC droplets that were printed into each of the short-pitch CLC droplets.

used as the printing substrate and the other as a top substrate. These were chosen as they promote a planar alignment of the LC director at the substrate boundary. Bursts of 30 droplets were jetted from an 80  $\mu\text{m}$  piezoelectric nozzle (MJ-AT-01-80), held at 70  $^{\circ}\text{C}$ , and printed to form a grid (10  $\times$  15 grid with 500  $\mu\text{m}$  drop spacing). The final footprint diameter of the sessile droplets was 369  $\mu\text{m}$ .

The printed CLC samples were then transferred to a bespoke inkjet printer constructed in-house and fitted with an identical 80  $\mu\text{m}$  piezoelectric nozzle (MJ-ABP-01-80), driven by a waveform generator (Jet-Drive III MicroFab Technologies Inc.), as shown in Fig. 2a. The NLC was then supplied to the dispenser with a syringe, controlled with a screw to ensure a flat meniscus at the printhead. The printhead was held at a constant temperature of 70  $^{\circ}\text{C}$  by a closed-loop heater controller.

To verify the correct jetting of droplets from the nozzle, stroboscopic shadowgraphy imaging was used. Illumination was provided by a green LED (Luminus Devices PT-120-RAX-L15-MPK, DK-136M – 1), and captured by a lens (Krontech Microscope Lens) and a CCD camera (DFK 23U274, The Imaging Source) (see example shadowgraphy image in Step i) of Fig. 1). A high-speed camera (a colour Phantom Miro LAB 310) was used to observe the droplet impact and coalescence dynamics on the substrate in transmission. To position the light source (Photofluor II, 89 North) such that it was in-line with the high-speed camera's sensor for shadowgraphy, the nozzle was not placed perpendicular to the substrate, as is typical in most DoD experiments. Instead, a custom machined printhead held the nozzle at an angle of 30 $^{\circ}$  to the substrate normal, permitting immediate in-situ observation of the transmission of the droplet during the impact process, without the need to transfer samples to a separate observation system.

In combination with a custom x-y translation stage, the camera was used to direct the nozzle towards the centre of the sessile CLC droplets. Depending on the desired level of dilution and thus the final pitch (and consequently the desired reflected colour), the nozzle was then triggered to jet a droplet of NLC between 1 and 30 times into the sessile CLC droplet (Step ii) in Fig. 1. To assemble the device, the droplets were then brought in contact with top substrate (second identical substrate), separated by 20  $\mu\text{m}$  spacers with planar rubbed alignment layers faced each other and secured together by using a rapid epoxy adhesive (from Araldite) at room temperature (Step iii) in Fig. 1). By this stage, the CLC/NLC droplets had largely mixed, but to ensure full diffusion, the samples were then transferred to an oven for 10 min at 80  $^{\circ}\text{C}$  (Step iv) in Fig. 1). Observations under the microscope confirmed that this had led to satisfactory diffusion of the jetted NLC into the printed CLC droplet.

Fig. 2b presents sessile CLC droplets, of which a subset has been doped with NLC droplets. The bottom rows exhibit colour variation as a result of the addition of the NLC. The number of supplementary printed NLC droplets ranges between 0 and 29. The blue reflection observed in the majority of the droplets is indicative of the undiluted short-pitch CLC. It is important to note that these droplets are not encapsulated by a top substrate, nor were they exposed to any thermal treatment.

It is evident that the addition of NLC droplets, in contrast to the short-pitch CLC, alters the reflection colour of the droplets, transitioning from blue to greenish and eventually to orangish hues. However, a closer examination reveals a colour gradient across the droplet, which is likely attributable to poor mixing at room temperature. This observation will be further discussed in the subsequent section. The inset image in Fig. 2b shows the photonic bandgap/reflection band for the undiluted CLC ink composition, droplets of which were formed using this CLC as an ink.

### 3. Results and discussion

#### 3.1. Jetting NLC ink into sessile CLC droplets

For inkjet-printed LC droplets, the timescales of the jetting process are much shorter than the timescales of the director alignment and general nematodynamics [32]. The jetting dynamics can be seen in Fig. 3a, which shows the arrival, impact, and coalescence of a single NLC

droplet (inflight diameter  $69 \pm 3 \mu\text{m}$ ) into a sessile CLC droplet (base diameter 369  $\mu\text{m}$ ). The nematic LC droplet rapidly decelerates on impact with the CLC droplet, with its momentum quickly dissipating due to viscosity. After the first few milliseconds, as the high-speed imaging reveals, the NLC fluid is confined to a small volume within the combined droplet (see the 25 ms and 75 ms frames in Fig. 3a). After 500 ms, the NLC fluid is barely visible in the last image of Fig. 3a, indicating that the fluid has recoiled to the top (in the side view) of the combined droplet, close to the impact site. In particular, there is little stretching and folding of the internal interface that can improve the efficiency of mixing by reducing the length scale over which diffusion must occur [34]. Therefore, the NLC must be left to slowly mix by molecular diffusion with the CLC over the length scale of the entire droplet ( $L \sim 300 \mu\text{m}$ ), without any significant contribution of advection. This observation is in agreement with the literature for similarly sized inkjet printed droplets, where if the impacting and sessile droplets have similar sizes and properties, advection does not significantly improve the efficiency of mixing [35].

As both impacting and sessile droplets are based largely the same composition (namely E7), we can approximate their diffusion coefficient by that of 5CB (the majority component of E7), which is  $D = 10^{-10} \text{ m}^2 \text{ s}^{-1}$  [36]. The time required for the NLC droplet to diffuse over the required length scale  $L \sim 300 \mu\text{m}$  can be estimated as  $t = L^2/D$ , which is on the order of  $10^3 \text{ s}$  [37]. This estimation is supported by Fig. 3b, where approximately half the combined droplet appears mixed after 300 s (i.e., across a length of  $\sqrt{tD} \sim 170 \mu\text{m}$ ). As  $D$  typically increases with temperature [38], approximately 10 min of mixing in the oven should be sufficient to mostly homogenise the combined droplet. Because the primary mixing mechanism is diffusion over long length scales, the exact impact location and angle of the NLC droplet do not greatly affect the composition of the final droplet. However, to ensure the final mixed droplet's position remains concentric with the original CLC droplet's centre, the NLC droplets were targeted to impact the centre of the sessile CLC droplet.

Fig. 4 presents the results of the alignment quality and appearance of reflection colours inside the droplets. The alignment of the helicoidal CLC domains showed asymmetry when viewed from the top and bottom substrates as schematically illustrated in Fig. 4a and experimentally shown in Fig. 4b. The optical microscope images suggest that the chiral structure adjacent to the bottom substrate is close to an ideal Grandjean texture while the top-down texture is less uniform, particularly near the centre of the image. This difference may be due to topological incompatibility between the LC molecules' surface alignment at the LC-air interface (homeotropic, promoting focal-conic configuration) and the alignment induced by contact with the rubbed PI layer (promoting a more ideal helix alignment), together with the influence of the dynamics of the wetting process when the top substrate is placed on the device. The misalignment, however, has little discernible effect on the light reflection properties of the assembled droplets. Since most reflected light comes from the first few pitches of the helicoidal structure, imperfections in the director field alignment near the top substrate do not affect the device's performance when viewed from below. Moreover, the free-standing droplet images of the longer pitch green and red CLC droplets suggest that the NLC is completely diffused and exhibits green and reddish reflection hues, just like the short-pitch (blue) CLC droplet (see Fig. 4c).

Regarding droplet sizes before and after device assembly, the footprint diameter of the short-pitch CLC droplet (without NLC added) was 369  $\mu\text{m}$ . The diameter of the CLC droplets after depositing 10 and 20 NLC drops was 407  $\mu\text{m}$  and 439  $\mu\text{m}$ , respectively. Similarly, the diameter of the short pitch blue colour droplet (without NLC droplet being added) after the addition of the top substrate and thermal mixing in the oven was found to be 355  $\mu\text{m}$ . Finally, the diameter of the CLC droplets after depositing 10 and 20 NLC drops and after the addition of the top substrate and thermal mixing in the oven was found to be 378  $\mu\text{m}$  and 416  $\mu\text{m}$ , respectively.



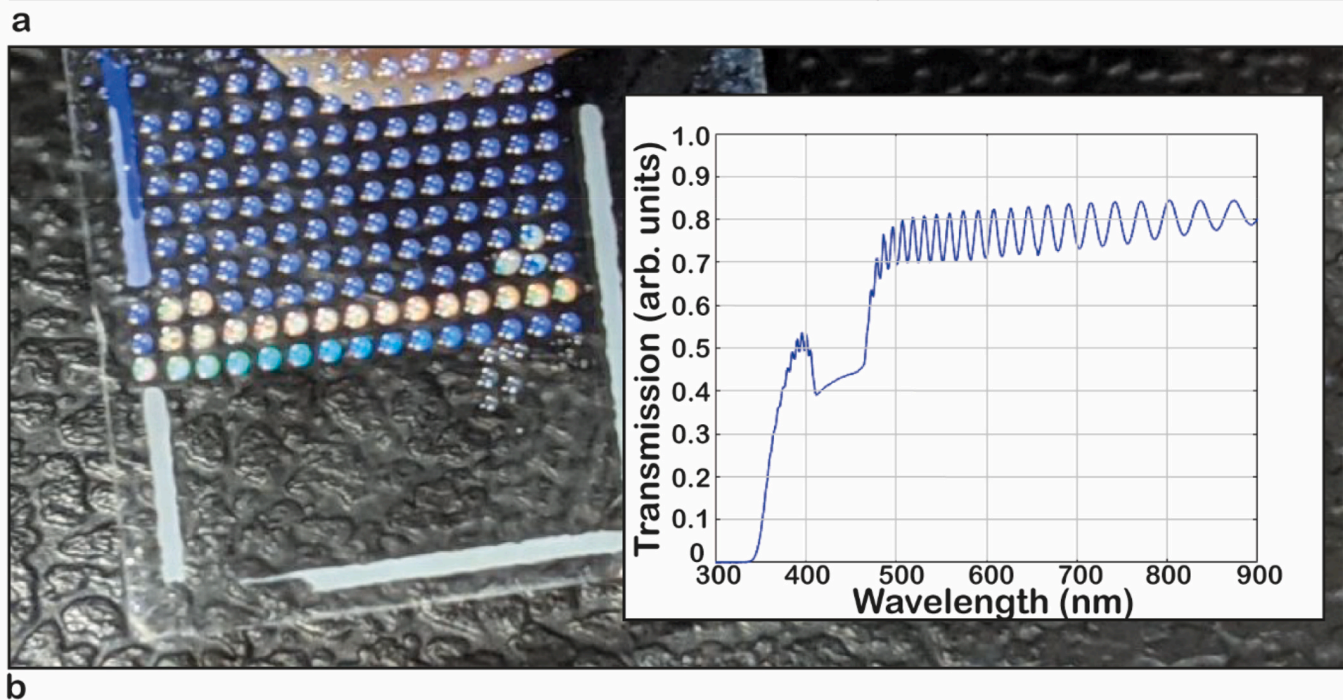
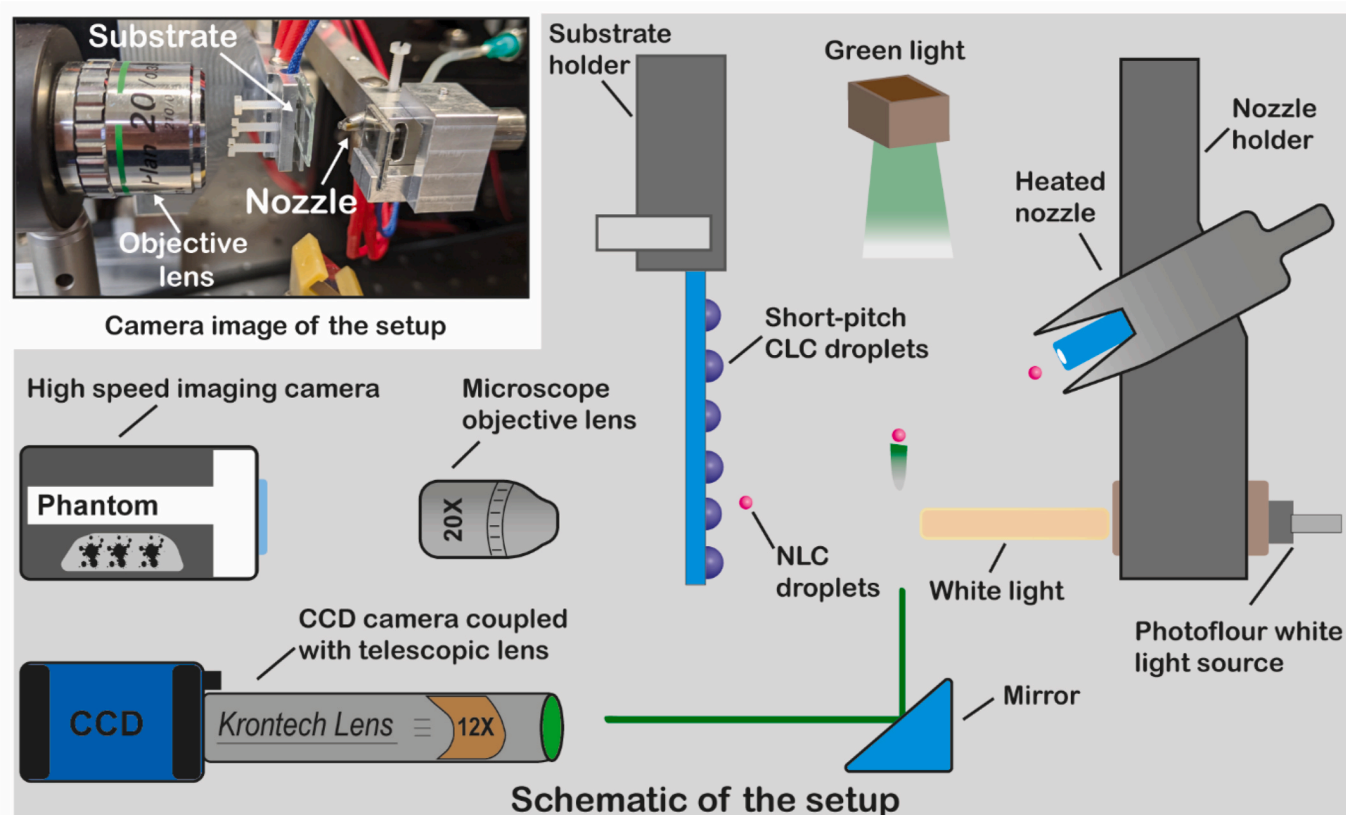


**Fig. 2.** Printing system and examples of printed CLC/NLC arrays. a). Schematic diagram showing the experimental setup used to deposit NLC droplets into already printed CLC droplets. The experiment also enables visual inspection of the drop impact using a high-speed camera. The inset in the top left is a photograph of the actual experimental arrangement. b) Photograph showing an example of an array of printed CLC droplets whereby the reflected colour has been tuned through the deposition of the NLC at different concentrations so as to elongate the pitch. The droplets that show a blue reflection were printed using a CLC ink formulation of 4.7 wt% chiral dopant (BDH1281) in the NLC host, E7. These blue droplets were printed using a MicroFab Jetlab II inkjet printer. The inset image shows the transmission spectrum for white light for this CLC mixture with a band-gap centered at around  $\lambda = 435$  nm when filled into a glass cell and observed on a UV-Vis Spectrometer at room temperature.

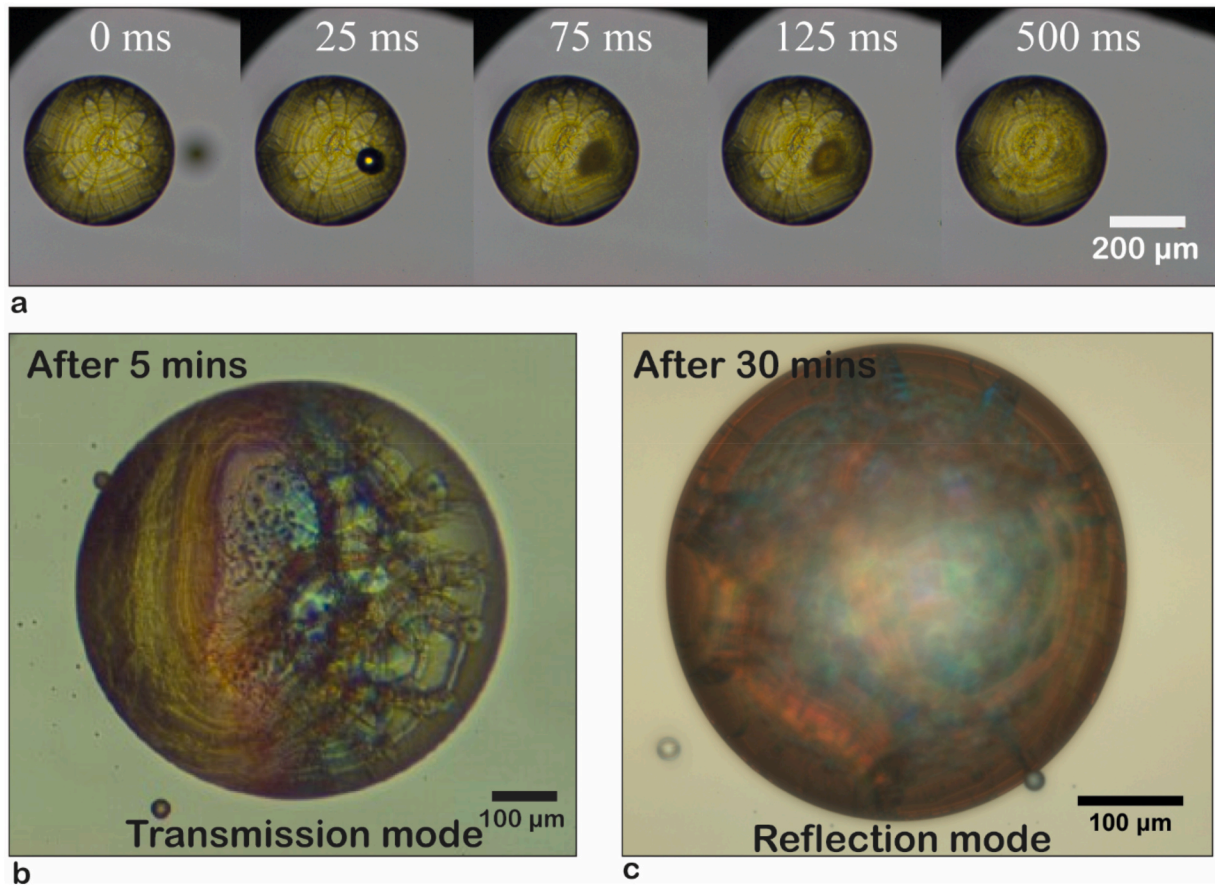


**Fig. 3.** Coalescence of printed NLC and CLC droplets. a). Series of images captured using a high-speed camera as the NLC droplets impact a printed short pitch CLC droplet. The image shows the inflight motion and deposition process of a NLC droplet. b). A high-speed camera frame when 20 NLC droplets were injected into an already printed short pitch CLC droplet. The image was taken after 5 min following the printing process. c). optical microscope image of the droplet as shown in (b) 30 min after the printing process. The image shows a mostly mixed NLC in a CLC droplet. The image was taken in reflection mode on an optical microscope.

### 3.2. Analysis of the pitch tuning

In this section, we demonstrate the link between the experimentally observed pitch lengthening, and the theoretical change in chiral pitch that would result from the dilution of the CLC by the NLC. The theoretical helical twisting power of a doped LC mixture scales linearly with its concentration, and thus inversely with volume. Therefore, the new chiral pitch of a mixture that has been diluted from volume  $V_0$  to  $V_1$  by the addition of a NLC may be found as  $p_{new} = \frac{V_1}{V_0} \times p_{old}$ , where  $p_{old}$  is the pitch of the original non-diluted CLC mixture which is 269 nm. The ratio  $\frac{V_1}{V_0}$  was measured from side profile images of the droplets, assuming they all wet to spherical caps of the same contact angle.

To experimentally measure the reflection spectra of the pitch-varied droplets, as shown in the optical microscope images in Fig. 5a, a USB spectrometer (Ocean Optics 2000+) was connected to the phototube of an Olympus BX51 microscope equipped with a reflection arm. The experimental arrangement of recording reflection spectra is shown Fig. S1 in the supplementary information. The theoretical reflection spectrum of an ideal chiral reflector is a rectangular bandgap, with edges located at wavelengths given by  $\lambda_o = n_o P$  and  $\lambda_e = n_e P$ , and the midpoint being  $\bar{n}P$  where  $\bar{n} = \frac{n_o + n_e}{2}$  and  $n_o$  and  $n_e$  are the ordinary and extraordinary refractive indices, respectively. In practice, the measured reflection spectra shown in Fig. 5b are not rectangular but approximately Gaussian in shape due to limitations in our spectroscopy technique and droplet configuration. To find their midpoints, a Gaussian fit was used, with the midpoint of the Gaussian taken to be  $\bar{\lambda}$ . From that, the bandgap edges  $\lambda_e$  and  $\lambda_o$  were derived from the fitted  $\bar{\lambda}$  as  $\lambda_e = \frac{\bar{\lambda} n_e}{\bar{n}}$  and

$$\lambda_o = \frac{\bar{\lambda} n_o}{\bar{n}}.$$

Fig. 6 shows a comparison of the theoretical and actual bandgaps, calculated using the methods described above. We note there is a generally good agreement between the increasing theoretical and actual bandgaps. However, the theoretical bandgap diverges from the measured bandgap as the number of added NLC droplets increases. This is likely a consequence of issues with estimating the volume of the droplets from microscopy. These could range from not accounting for the Bond number of the samples, which increases as the droplets become larger, to small inhomogeneities in the fluid mixing near the boundaries. This is an acceptable deviation, as a calibration curve may still be established between the number of NLC drops  $N$  and the resultant reflection band centre  $\lambda$  which would be perfectly acceptable in an industrial context.

Furthermore, it can be noted that the reflected colours from the printed CLC droplets are generally temperature dependent. This dependence is because the pitch of the helicoidal structure elongates or contracts depending on the type of chiral dopant used and the temperature dependent elastic properties of the nematic LC host [39]. In the case of our on-demand pitch-varying method, we can therefore thermally induce variations in the pitch in each individual CLC droplet, leading to the reflection of different colours.

### 3.3. Printed colour images

Finally, we conclude by demonstrating how this technique could be used to create colour graphics. Fig. 7 presents an example of a printed array of short-pitch CLCs that have been ‘tuned’ to different colours by



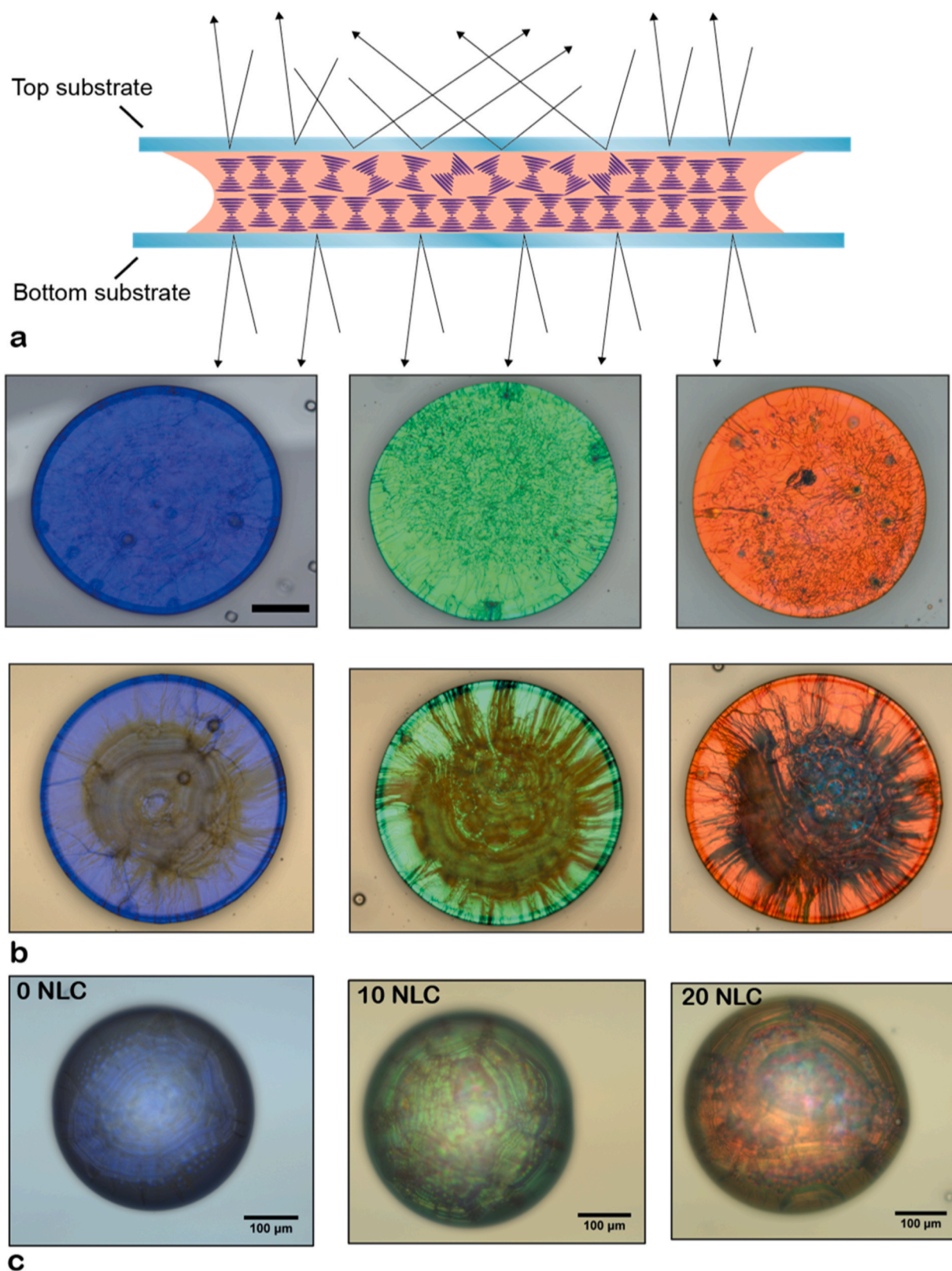


**Fig. 4.** Blue-Green-Red CLC droplets by tuning with NLC printed droplets. a). Graphical illustration to demonstrate the arrangement of the helicoidal CLC domains and the reflection of light when viewed from the top and bottom substrates. The domains are represented in the form of intrinsic helical structures. b). Optical microscope images of the droplets when sandwiched between two glass substrates with planar alignment layers. The images on the first row correspond to the case when viewed from the bottom substrate. The scale bar is equal to 75  $\mu\text{m}$ . The images in the second row correspond to the case when viewed from the top substrate side of the cell. The blue coloured droplet corresponds to the case when no NLC droplet was deposited. The green and orange/red coloured droplets, on the other hand, correspond to the case when 10 and 20 NLC droplets were deposited into short pitch CLC droplets, respectively. c). Optical microscope images of free-standing CLC droplets when diluted with NLC droplets before the addition of the top substrate. The numbers in black over each droplet corresponds to the number of NLC droplets being deposited. The images were taken prior to attaching the top substrate.

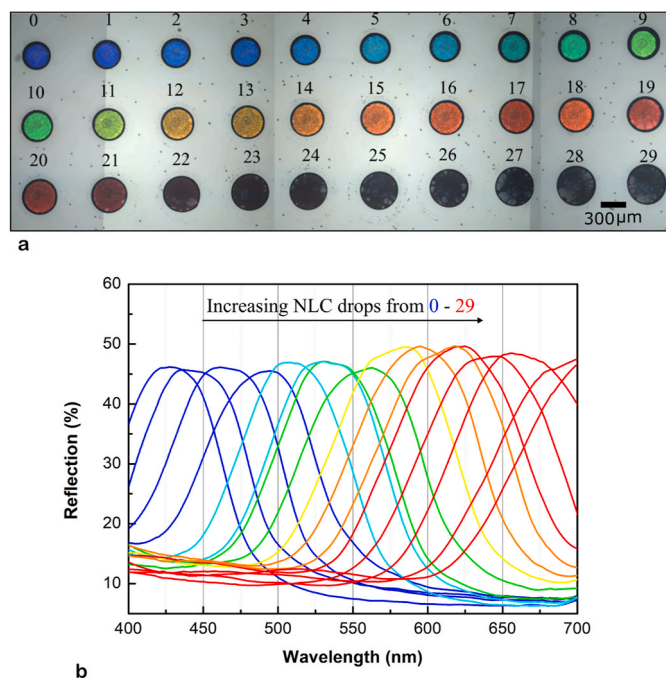


**Fig. 5.** Tuning the CLC pitch. a). Optical microscope image shows different coloured CLC reflectors fabricated by tuning the pitch through a two-step printing process, as shown in Fig. 1. Step 1- printing short-pitch CLC as an ink in the form of sessile droplets. The droplets reflect blue light. Step 2 - printing NLC droplets into the short pitch CLC droplets to increase the pitch and hence reflect light of different colours. The numbers in black above each droplet correspond to the number of NLC droplets that were deposited onto each of the already printed CLC droplets. b). The plot shows the reflection spectra for each of the different CLC reflectors presented in (a). Reflection spectra were captured using an Ocean Optics USB 2000+ spectrometer connected to the phototube of an optical microscope with a reflection arm.

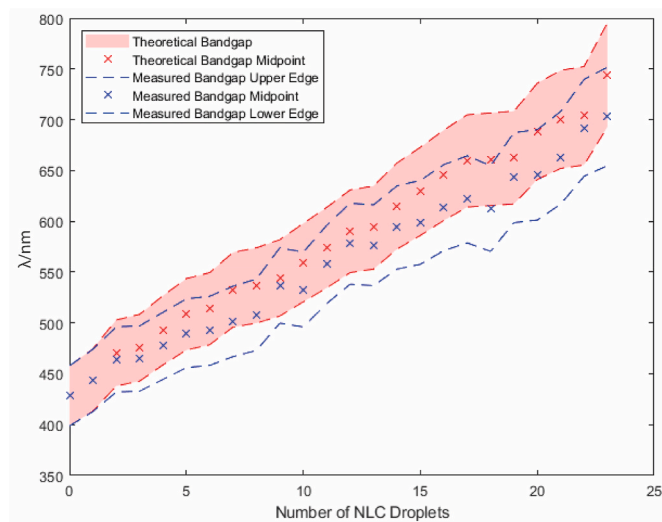


**Fig. 6.** Dependence of the reflection band on the number of printed NLC droplets. Plot of the central wavelength of the reflection band,  $\lambda$ , as a function of the number of printed NLC droplets. Results are presented for the theoretical bandgap that was estimated by considering the droplet volume and the measured bandgap from the spectra presented in Fig. 5.

printing a predefined number of droplets of NLC into the sessile CLC droplets. Through precise control of the NLC deposition, we successfully formed the alphanumeric characters ‘SMP’ as shown. In Fig. 7b, we

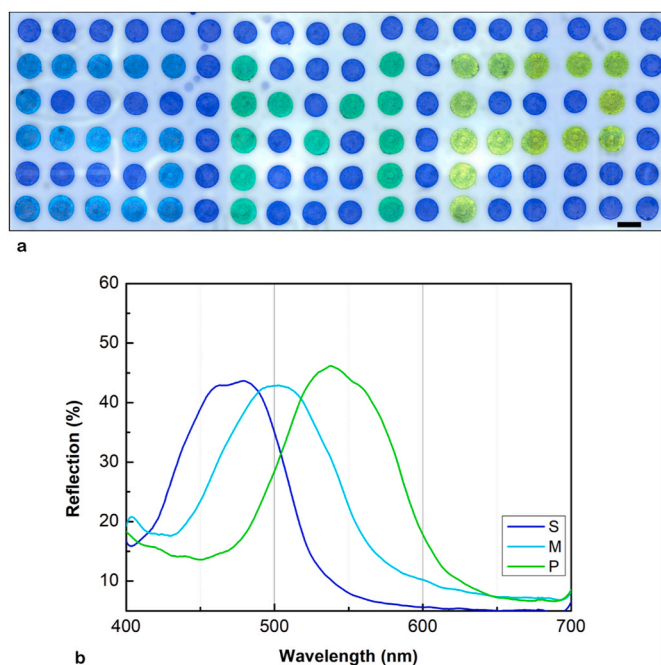


**Fig. 7.** Printed coloured alphanumeric characters by tuning the pitch with a NLC. a). Optical microscope image showing three alphanumeric characters ‘SMP’ that were fabricated by inkjet printing NLC droplets (of differing amounts) into printed CLC droplets. The black scale bar in the bottom right corner is 300  $\mu\text{m}$ . b). The plot shows the reflection spectra for each of the three different coloured CLC reflectors presented in the ‘SMP’ characters in (a).

display the corresponding reflection spectra for the resulting droplets in the S, M, and P characters. In our study, we also examined the stability of the optical texture and the reflected colours from the printed CLC droplets over an extended period of time, considering long-term applications for printed CLC based devices. The results revealed no changes in the optical texture or reflection colours over time, indicating a high level of stability.

#### 4. Conclusions

In this work, a method for tuning the pitch of printed CLC droplets has been demonstrated by depositing picolitres of nematic LC droplets into short-pitch CLC droplets using drop-on-demand inkjet printing. The results show that by increasing the number of printed NLC droplets from 0 to 29 the centre of the CLC reflection band can be tuned from  $\lambda \sim 430$  nm to  $\lambda > 700$  nm. Results indicate that mixing of the NLC and CLC droplets occurs in timescales of the order of 10 min, which is in reasonable agreement with estimates of the diffusion time based on the diffusion coefficient of the nematic LC 5CB, which is one of four components in the eutectic nematic LC mixture used in this study. Furthermore, we have considered the dependence of the measured reflection bandgap on the number of printed NLC droplets, which compares well with the dependence of the theoretical bandgap on the number of printed droplets. To conclude, we have demonstrated how this approach of tuning CLC droplets using printing can be used to form images/graphics on-demand through the demonstration of a printed coloured logo. In the future, it would be interesting to investigate on-demand mixing of a wider range of LC parameters, for example materials with differing optical anisotropies ( $\Delta n$ ) could be used to further achieve variation in the width of the reflection band gap to control the colour purity. Additionally, it would also be interesting to investigate how the colour properties of the printed droplet arrays could be dynamically tuned, for example through the application of electric fields via electrodes integrated into the device structure.



## Credit author statement

Conceptualization: WK, ACJO, AACP, SJE, SMM, Methodology: WK, ACJO, TCS. AACP, SJE, SMM, Validation: WK, ACJO, TCS, Formal analysis: WK, ACJO, TCS, Investigation AACP, SJE, SMM, Resources AACP, SJE, SMM, Data Curation: WK, ACJO, TCS, Writing - Original Draft: WK, ACJO, TCS Writing - Review & Editing: AACP, SJE, SMM, Supervision: AACP, SJE, SMM, Project administration: AACP, SMM, Funding acquisition: AACP, SJE, SMM.

## Declaration of competing interest

The authors declare that they have no known competing financial interests or personal relationships that could have appeared to influence the work reported in this paper.

## Data availability

Data will be made available on request.

## Acknowledgments

W.K. acknowledges the financial support provided by Punjab Educational Endowment Fund (PEEF), Pakistan. A.C.J.O. acknowledges the Engineering and Physical Sciences Research Council for a graduate studentship (EP/R513295/1). A.A.C-P was supported by The Royal Society through a University Research Fellowship (URF\R\180016) and the John Fell Fund, Oxford University Press, via a Pump-Priming grant (0005176).

## Appendix A. Supplementary data

Supplementary data to this article can be found online at <https://doi.org/10.1016/j.mtadv.2023.100416>.

## References

- [1] J.W. Goodby, Chirality in liquid crystals, *J. Mater. Chem.* 1 (1991) 307.
- [2] P. G. de Gennes, J. Prost, *The Physics of Liquid Crystals*, 1993, p. 616.
- [3] H.K. Bisoyi, Q. Li, Light-driven liquid crystalline materials: from photo-induced phase transitions and property modulations to applications, *Chem. Rev.* 116 (2016) 15089–15166.
- [4] U.A. Hrozhyk, S.V. Serak, N.V. Tabiryan, T.J. Bunning, Optical tuning of the reflection of cholesterics doped with azobenzene liquid crystals, *Adv. Funct. Mater.* 17 (2007) 1735–1742.
- [5] J. Ma, Y. Li, T. White, A. Urbas, Q. Li, Light-driven nanoscale chiral molecular switch: reversible dynamic full range color phototuning, *Chem. Commun.* 46 (2010) 3463.
- [6] I. Dierking, Chiral liquid crystals: structures, phases, effects, *Symmetry (Basel)* 6 (2014) 444–472.
- [7] C.R. Smith, D.R. Sabatino, T.J. Praisner, Temperature sensing with thermochromic liquid crystals, *Exp. Fluid* 30 (2001) 190–201.
- [8] J. Chen, S.M. Morris, T.D. Wilkinson, H.J. Coles, Reversible color switching from blue to red in a polymer stabilized chiral nematic liquid crystals, *Appl. Phys. Lett.* 91 (2007), 121118.
- [9] F.J. Kahn, Electric-field-induced color changes and pitch DILATION in cholesteric liquid crystals, *Phys. Rev. Lett.* 24 (1970) 209–212.
- [10] H. Xianyu, S. Faris, G.P. Crawford, In-plane switching of cholesteric liquid crystals for visible and near-infrared applications, *Appl. Opt.* 43 (2004) 5006.
- [11] O.T. Picot, et al., A real time optical strain sensor based on a cholesteric liquid crystal network, *RSC Adv.* 3 (2013), 18794.
- [12] P. Cicuta, A.R. Tajbakhsh, E.M. Terentjev, Evolution of photonic structure on deformation of cholesteric elastomers, *Phys. Rev. E* 65 (2002), 051704.
- [13] K. Yao, Q. Meng, V. Bulone, Q. Zhou, Flexible and responsive chiral nematic cellulose nanocrystal/poly(ethylene glycol) composite films with uniform and tunable structural color, *Adv. Mater.* 29 (2017), 1701323.
- [14] A. Saha, et al., Irreversible visual sensing of humidity using a cholesteric liquid crystal, *Chem. Commun.* 48 (2012) 4579.
- [15] D.A. Winterbottom, R. Narayanaswamy, I.M. Raimundo, Cholesteric liquid crystals for detection of organic vapours, *Sensor. Actuator. B Chem.* 90 (2003) 52–57.
- [16] A. Mujahid, H. Stathopoulos, P.A. Lieberzeit, F.L. Dickert, Solvent vapour detection with cholesteric liquid crystals—optical and mass-sensitive evaluation of the sensor mechanism, *Sensors* 10 (2010) 4887–4897.
- [17] C.-K. Chang, C.W.M. Bastiaansen, D.J. Broer, H.-L. Kuo, Discrimination of alcohol molecules using hydrogen-bridged cholesteric polymer networks, *Macromolecules* 45 (2012) 4550–4555.
- [18] D. Wang, S. Nam, W. Jung, H.J. Yang, S.S. Choi, Electrically wavelength-controllable color filters with high optical transmittance using heterogeneous chiral liquid crystals, *Adv. Opt. Mater.* n/a (2023), 2202906.
- [19] S.M. Wood, S.J. Elston, S.M. Morris, Wavelength-tuneable laser emission from a dye-doped achiral nematic liquid crystal dispersed into a chiral polymer scaffold, *Mol. Cryst. Liq. Cryst.* 632 (2016) 89–96.
- [20] D.J. Mulder, A.P.H.J. Schenning, C.W.M. Bastiaansen, Chiral-nematic liquid crystals as one dimensional photonic materials in optical sensors, *J. Mater. Chem. C* 2 (2014) 6695–6705.
- [21] S. Nam, D. Wang, G. Lee, S.S. Choi, Broadband wavelength tuning of electrically stretchable chiral photonic gel, *Nanophotonics* 11 (2022) 2139–2148.
- [22] M. Stebryte, Reflective optical components based on chiral liquid crystal for head-up displays, *Liq. Cryst. Today* 30 (2021) 36–45.
- [23] S.M. Morris, et al., Optically activated shutter using a photo-tunable short-pitch chiral nematic liquid crystal, *Appl. Phys. Lett.* 103 (2013), 101105.
- [24] H.-K. Kwon, et al., Optically switchable smart windows with integrated photovoltaic devices, *Adv. Energy Mater.* 5 (2015), 1401347.
- [25] D.J. Gardiner, et al., Printed photonic arrays from self-organized chiral nematic liquid crystals, *Soft Matter* 8 (2012) 9977–9980.
- [26] W. Kamal, et al., Spatially patterned polymer dispersed liquid crystals for image-integrated smart windows, *Adv. Opt. Mater.* 2101748 (2021), 2101748.
- [27] M. Li, et al., Printed polymer-stabilized chiral nematic liquid crystal privacy windows, *Macromol. Chem. Phys.* 223 (2022), 2200154.
- [28] M. Moirangthem, A.F. Scheers, A.P.H.J. Schenning, A full color photonic polymer, rewritable with a liquid crystal ink, *Chem. Commun.* 54 (2018) 4425–4428.
- [29] J. Yang, et al., Printable photonic polymer coating based on a monodomain blue phase liquid crystal network, *J. Mater. Chem. C* 7 (2019) 13764–13769.
- [30] M. Moirangthem, A.P.H.J. Schenning, Full color camouflage in a printable photonic blue-colored polymer, *ACS Appl. Mater. Interfaces* 10 (2018) 4168–4172.
- [31] L. Zhang, et al., Spatial patterning of fluorescent liquid crystal ink based on inkjet printing, *Molecules* 27 (2022) 5536.
- [32] E. Parry, S. Bolis, S.J. Elston, A.A. Castrejón-Pita, S.M. Morris, Drop-on-Demand inkjet printing of thermally tunable liquid crystal microlenses, *Adv. Eng. Mater.* 20 (2018), 1700774.
- [33] W. Kamal, et al., Electrically tunable printed bifocal liquid crystal microlens arrays, *Adv. Mater. Interfac.* 7 (2020), 2000578.
- [34] T.C. Sykes, et al., Surface jets and internal mixing during the coalescence of impacting and sessile droplets, *Phys. Rev. Fluids* 5 (2020), 023602.
- [35] J.R. Castrejón-Pita, K.J. Kubiak, A.A. Castrejón-Pita, M.C.T. Wilson, I. M. Hutchings, Mixing and internal dynamics of droplets impacting and coalescing on a solid surface, *Phys. Rev. E* 88 (2013), 023023.
- [36] M. Vilfan, et al., Surface-induced order and diffusion in 5CB liquid crystal confined to porous glass, *Magn. Reson. Imaging* 19 (2001) 433–438.
- [37] M.C. Wilson, J.R. Castrejón-Pita, A.A. Castrejón-Pita, *Reactive Inkjet Printing*, Royal Society of Chemistry, 2017, <https://doi.org/10.1039/9781788010511>.
- [38] S.J. Blundell, K.M. Blundell, *Concepts in Thermal Physics. TA - TT*, Oxford University Press, 2010. LK -, <https://worldcat.org/title/495270110>.
- [39] W. Zhang, et al., Temperature-responsive photonic devices based on cholesteric liquid crystals, *Adv. Photonics Res.* 2 (2021), 2100016.